

Adsorption equilibrium, kinetics and mechanism of Pb(II) over carbon–silica composite biosorbent with designed surface oxygen groups

Yuan Fan¹ · Shangru Zhai¹ · Na Liu¹ · Jialiang Lv¹ · Zhimin Lei¹ · Qingda An¹

Received: 31 January 2015 / Accepted: 11 April 2015 / Published online: 30 April 2015
© Springer Science+Business Media Dordrecht 2015

Abstract Heavy metal contamination, especially contamination involving Pb(II), is a major environmental problem faced by modern society; hence, research on bio-adsorbents with a low cost and high efficiency for removal of Pb(II) from water is highly desirable. Herein, a novel carbon–silica bio-sorbent prepared by carbonization of rice husk with sulfuric acid followed by ammonium persulfate oxidation was successfully applied to highly efficient Pb(II) removal. The synthetic adsorbent was characterized by scanning electron microscopy, Nitrogen (N₂) sorption, Fourier transform infrared and X-ray photoelectron spectroscopy techniques. Batch experiments with varying solution pH, contact time, temperature and ionic strength were carried out to evaluate the adsorption performance. Adsorption equilibrium was achieved within 30 min, and adsorption kinetics were best fit by the pseudo-second-order model. The experimental data fitted the Langmuir isotherm better than the other two isotherms. Thermodynamic studies suggested that the adsorption process was spontaneous and endothermic. Furthermore, desorption results showed that adsorption performance can be retained at levels up to 80 % after being used four times. Overall, waste rice husk-derived carbon–silica composite bio-sorbent is an attractive candidate for the removal of Pb(II) from aqueous systems.

Electronic supplementary material The online version of this article (doi:[10.1007/s11164-015-2060-z](https://doi.org/10.1007/s11164-015-2060-z)) contains supplementary material, which is available to authorized users.

✉ Shangru Zhai
zhairs@dlpu.edu.cn

Na Liu
liu_na@dlpu.edu.cn

Qingda An
anqingda@dlpu.edu.cn

¹ Faculty of Light Industry and Chemical Engineering, Dalian Polytechnic University, Dalian 116034, China

Keywords Carbon–silica composite · Chemical modification · Bio-sorbents · Pb(II) removal · Oxygen-containing group

Introduction

Nowadays, with rapid modernization and industrialization, water pollution by toxic heavy metals has received worldwide attention. Among the heavy metals, lead is one of the most toxic elements, even at low concentrations. It affects the central nervous system, kidneys, liver, and gastrointestinal system, and it may directly or indirectly cause diseases such as anemia, encephalopathy, hepatitis, and nephritic syndrome [1]. Various industrial activities such as battery manufacturing, metal processing and mining have become the main source of lead-contaminated water. Thus, efficient removal of Pb(II) is of utmost importance to meet the increasing demand for clean water, especially in the region of Asia.

Numerous methods have been developed to treat lead-polluted water, including precipitation [2], electroplating [3], ion exchange [4], membrane separation [5], coagulation [6], and adsorption [7], etc. However, most of these methods have some inherent limitations, such as high operational costs, incomplete metal removal and generation of secondary wastes. Compared to other methods, adsorption has been found to be the most effective method as it offers low cost, easy operation, high efficiency and good reusability. Meanwhile, growing attention has been focused on the utilization of agricultural wastes or by-products as adsorbents for the elimination of heavy metals from wastewater due to their low cost and availability. Up to now, many kinds of adsorbents such as wheat bran [8], fruit waste [9], mansonia wood sawdust [10], lichen (*Parmelina tiliaceae*) biomass [11], macrofungus (*Lactarius scrobiculatus*) biomass [12], and macrofungus (*Amanita rubescens*) biomass [13], have been introduced for Pb(II) removal.

Agricultural residues, especially rice husk, a by-product of the rice milling industry, accounts for about 20 % of whole rice [14]. It mainly consists of cellulose, lignin, hemicelluloses and silica [15]. Recently, the global consumption of rice has been 470 million metric tons [16]; thus, several million tons of rice husk have been produced, posing a disposal problem. Generally, most of the waste husks are discarded or burned without proper utilization, which is unfavorable to the environment [17]. In light of these facts, development of treatment approaches that facilitate the utilization of rice husk is a pressing need. Consequently, significant efforts have been devoted to the application of rice husk in many fields such as fuel production [18–20], fertilizers [21], construction materials [22], catalytic supports [23], and capacitors [24], etc. More recently, however, Wong et al. [25] and Wang et al. [26] employed rice husk as a raw material for lithium ion battery-related applications. Thus, how to efficiently utilize rice husk is still an interesting topic. Importantly, adsorption using rice husk has been recognized as a promising method of removing heavy metal ions from aqueous solutions. It is worth noting that rice husk, with its granular structure, water insolubility, high chemical stability, and high mechanical strength, contains abundant floristic fiber, and some functional groups such as carboxyls, hydroxyls, and amidogens, which have natural adsorption

capacity for metal ions [27, 28]. But this capacity is low. As is well known, sorbents with proper functional groups play key roles in adsorption performance. Having favorable physical and chemical surface characteristics, various modifications on rice husk have been investigated by many researchers in order to enhance its sorption capacity [29–35]. However, these methods or prepared materials still suffer from drawbacks, such as use under high temperatures, use of alkali reagents or low adsorption capacities. What's more, directly utilizing rice husk to fabricate high-performance bio-sorbents that can rapidly remove Pb(II) has been rarely reported. Therefore, it is urgent to develop rice husk-based bio-sorbents with simple syntheses and high Pb(II) adsorption capacities.

Herein, in continuation of our research interest on rice husk-based bio-sorbents for dye removal from water [36, 37], a more facile route for the fabrication of rice husk-based carbon–silica composite bio-sorbents, which can efficiently remove Pb(II) from aqueous solution, has been developed. This carbon–silica composite bio-sorbent was prepared by employing a two-step method that firstly involved carbonization of rice husk with sulfuric acid, followed by adopting ammonium persulfate as an oxidant. This method may have some benefits. To begin with, contrary to traditional alkali extraction or activation processes, preparation is mild and simple, thereby saving energy and being environmentally benign; besides, during the sulfuric acid-assisted low-temperature carbonization, carbohydrate components of rice husks are broken into small molecules, leading to a carbonaceous material loaded with functional groups on the surface such as –COOH and –OH [38]. The presence of these functional groups made the materials more hydrophilic, which increases their further functionalization. Moreover, the use of rice husk-based bio-sorbents not only provides a feasible solution to reduce waste in an economic and eco-friendly way but also offers an efficient solution for lead pollution control. The synthetic adsorbent was characterized by scanning electron microscopy (SEM), N_2 sorption, Fourier transform infrared (FTIR) and X-ray photoelectron spectroscopy (XPS) techniques. Batch experiments were thoroughly employed to investigate the adsorption behaviors; impact factors, such as solution pH, contact time, temperature and ionic strength were examined. The adsorption kinetics, isotherms, thermodynamics and desorption experiments were also studied in detail.

Experimental

Materials

Rice husk was obtained from a rice mill near Dalian, Liaoning Province, China. It was washed by distilled water in order to remove adhering soil and dried in an oven at 100 °C over night, and then cut into 60 meshes. Lead nitrate ($Pb(NO_3)_2$) and sodium nitrate ($NaNO_3$) were purchased from Sinopharm Chemical Reagent Co., Ltd, China. Ammonium persulfate ($(NH_4)_2S_2O_8$) was purchased from Beijing J & K Chemical Technology Co., Ltd, China. Calcium chloride anhydrous ($CaCl_2$) was

purchased from Tianjin Kermel Co., Ltd, China. All chemical reagents used were analytical grade. De-ionized water was used throughout the experiment.

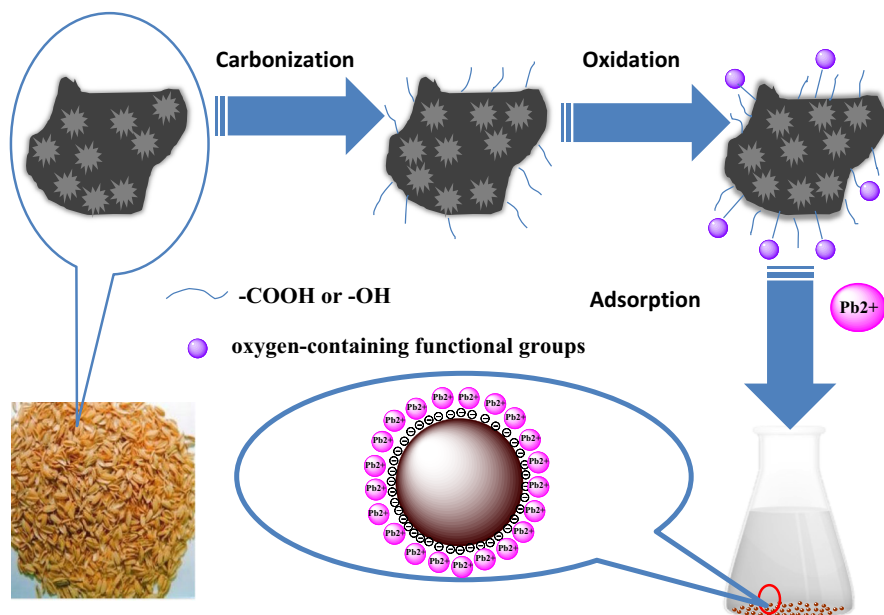
Preparation of carbon–silica bio-sorbent

Low-temperature aqueous carbonization

5.0 g of rice husk powder was placed in a glass beaker and 50 ml of 70 % (mass fraction) H_2SO_4 aqueous solution was added. The slurry was magnetically stirred for 10 min, and then loaded into a 120 mL sealed, Teflon-lined stainless steel autoclave for carbonization at 100 °C for 6 h. The black solid was filtrated through a sand core funnel, and washed repeatedly with distilled water until the wash water became neutral. Following filtration, the sample was dried at 100 °C for 24 h in a drying oven. This sample was denoted as RH-C.

Surface modification by oxidation treatment

3.0 g of RH-C impregnated with saturated solution of $(\text{NH}_4)_2 \text{S}_2\text{O}_8$ in 1 M H_2SO_4 (using a 1:10 solid to liquid ratio) was placed in a glass beaker and stirred at room temperature for 12 h. Then the product was collected by filtration and washed repeatedly with distilled water until the wash water become neutral. The sample was dried at 100 °C for 12 h and ground to powder. The resulting product was denoted



Scheme 1 Preparation and adsorption of Pb(II) onto the RH-C-ox with plentiful, accessible oxygen-containing functional sites on the surface

as RH-C-ox and used as the adsorbent. Correspondingly, Scheme 1 shows the preparation and adsorption process for Pb(II) onto the as-prepared RH-C-ox. The carbon–silica composite bio-sorbent can be prepared by a facile approach. First, rice husk was carbonized with sulphuric acid at low temperature to induce small polycyclic aromatic carbon sheets bearing hydroxyl and carboxyl groups; and then oxidation of the prepared samples resulted in small polycyclic aromatic carbon sheets containing oxygenous functional groups, which were primarily responsible for the sorption of Pb(II).

Characterization

The surface morphologies of RH-C and RH-C-ox were determined by SEM (SEM, JSM-6460LV, JEOL, Japan). FTIR (Perkin-Elmer, USA) spectra in the 4000–400 cm^{-1} region were acquired by using KBr pellets. XPS measurements were performed using a Thermo Scientific ESCALAB250 spectrometer (Thermo VG, USA) equipped with an Al-K α X-ray source (1486.6 eV). The specific surface area and pore diameter of the samples were determined by nitrogen adsorption–desorption experiments at a temperature of 77 K with an automated sorptometer (Quantachrome Autosorb NOVA2200e, USA).

Adsorption experiments

Adsorption of Pb(II) on RH-C-ox was performed by batch technique. Typically, 10 mg of the adsorbent was added to 20 mL of Pb(II) solution at various desired concentrations in 50-mL Erlenmeyer flasks. The suspensions were shaken at a constant speed (150 rpm) for 1.5 h.

The effect of solution pH on Pb(II) adsorption was studied in a pH range of 2–6 at room temperature. The initial pH of the 30 mg L^{-1} Pb(II) ion solutions was adjusted using 0.1 M HCl solution. The suspensions were shaken for 1.5 h. The pH was measured using a pH meter (pHS-3C, Shanghai, China).

The effect of contact time on Pb(II) adsorption was examined to analyze the adsorption kinetics at a pH of ~ 5 at room temperature. Assessment of adsorption kinetics of Pb(II) on RH-C-ox was conducted with 10, 25, and 40 mg L^{-1} Pb(II) ion solutions at different times varying from 1 to 80 min.

For isotherm studies, the adsorption of Pb(II) was conducted with initial concentrations ranging from 25 to 200 mg L^{-1} at 293, 303 and 313 K under the optimum pH value of 5 with continuous stirring for 1.5 h to reach equilibrium.

Additionally, the effect of ionic strength (0.01–0.1 M NaNO_3 and CaCl_2) on the adsorption process was studied with a Pb(II) concentration of 25 mg L^{-1} and equilibrium time of 1.5 h.

After adsorption, the samples were filtered through a 0.22- μm membrane filter. The residual concentration of Pb(II) was analyzed by atomic absorption spectroscopy (AAS HITACHI 180–80, Japan). The equilibrium adsorption capacity q_e (mg g^{-1}) and the percentage removal efficiency (%R) were calculated as follows:

$$q_e = \frac{(C_0 - C_e)V}{m} \quad (1)$$

$$\%R = \frac{(C_0 - C_e)}{C_0} \times 100\% \quad (2)$$

where C_0 and C_e (mg L^{-1}) are the initial and equilibrium Pb(II) concentrations in the aqueous solution, respectively; V (L) is the volume of the solution and m (g) is the sorbent mass.

Desorption experiments

For desorption studies, 10 mg of adsorbent was first contacted with 20 mL of 25-mg L^{-1} Pb(II) for 1.5 h at room temperature. Afterwards, the suspension was filtered and the Pb(II) concentration in the filtrate was analyzed by AAS, and then the adsorbents were agitated with 20 mL of 0.1-M HCl solution for 4 h. The adsorbents were collected by filtration, washed with distilled water, dried and then reused for the next cycle. The adsorption–desorption experiments were conducted four times.

Data analysis

All experiments were repeated in triplicate with averages used as the results; the standard deviations (SDs) of the triplicate experiments are denoted by the error bars. The kinetic and isotherm models were fitted by employing the linear fitting and non-linear fitting method. In addition, the models were also evaluated by the error functions, i.e., second-order corrected Akaike information criterion (AIC) [39, 40] and the SD [55]. Expressions of the error functions are given below:

$$\text{AIC} = N \times \ln\left(\frac{\text{RSS}}{N}\right) + 2P \quad (3)$$

$$\text{SD} (\%) = 100 \sqrt{\frac{\sum |(q_{\text{exp}} - q_{\text{cal}})/q_{\text{exp}}|^2}{N - 1}} \quad (4)$$

where P is the number of parameters in the model, N the number of data points, and RSS denotes the residual sum of squares from the fitted model. The preferred model is the one with the lowest AIC value. q_{exp} and q_{cal} (mg g^{-1}) are the experimental and calculated amount of Pb(II), respectively. If data from a model are similar to the experimental data, the SD (%) will be low.

Results and discussion

Characterization of surface chemistry

SEM images of the RH-C and RH-C-ox are shown in Fig. 1. Obviously, the surface morphology of RH-C is different from that of RH-C-ox. RH-C has a rough surface

with irregular pores; however, slight aggregation of the irregular particles that are covered with pores can also be observed in RH-C-ox, possibly resulting from a mild solution-phase reaction process. This finding indicates that the chemical modification process of surface oxidation treatment slightly altered the porosity and morphology of RH-C. Moreover, the nitrogen adsorption–desorption isotherms and pore size distributions of the samples are illustrated in Fig. 2 and the Brunauer–Emmett–Teller (BET) surface area analysis data are given in Table 1. As shown in Table 1, the specific surface area, average pore size and pore volume of RH-C-ox was calculated at $20.251 \text{ m}^2 \text{ g}^{-1}$, 6.883 nm and $0.055 \text{ cm}^3 \text{ g}^{-1}$, respectively, by means of the BET analysis and the Barrett–Joyner–Halenda (BJH) pore size and volume analysis method. Clearly, the porosity of RH-C is larger than that of RH, which indicates that the adopted low-temperature carbonization process led to development of porosity in the sample. However, the surface area of RH-C-ox was reduced in comparison with RH-C, further confirming the reduction of specific surface area was possibly due to surface modification of carbonized species using ammonium persulfate as the oxidizing agent, which is in agreement with the SEM images.

The FTIR spectra of RH, RH-C and RH-C-ox are compared in Fig. 3. The FTIR spectrum of RH is similar to that of previous studies [41, 42]. The 3435 and 2924 cm^{-1} bands are assigned to the stretching vibration of the $-\text{OH}$ and $\text{C}-\text{H}$, while the bands at 1720 and 1631 cm^{-1} are associated with the $\text{C}=\text{O}$ stretching vibration and aromatic ring vibration. A band is observed at 1095 cm^{-1} , which belongs to an $\text{Si}-\text{O}-\text{Si}$ bond. The bands at 793 and 459 cm^{-1} are attributed to an $\text{Si}-\text{O}$ bond. However, it should be observed that all samples displayed a similar backbone with varied intensities, due to the different chemical modification process. Particularly, the FTIR transmission spectrum of RH-C-ox changed obviously after oxidation. The peak at 3436 cm^{-1} is broader and the relative intensity between 1714 and 1633 cm^{-1} changed significantly, which is possibly due to the significant increment of the oxygen-containing functional groups after surface oxidation treatment.

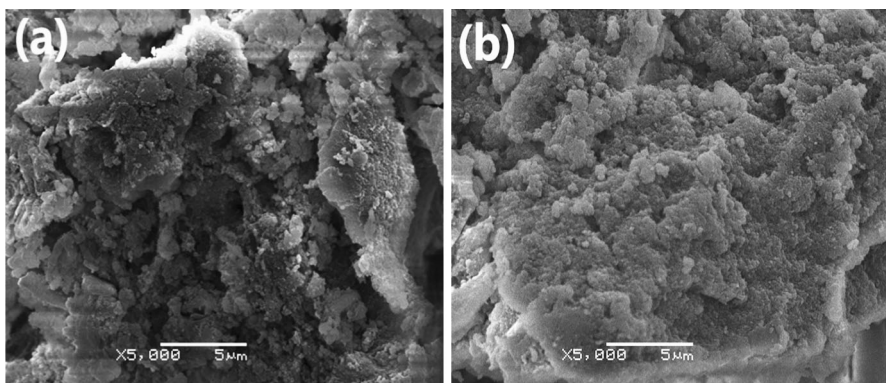


Fig. 1 SEM images of RH-C (a) and RH-C-ox (b)

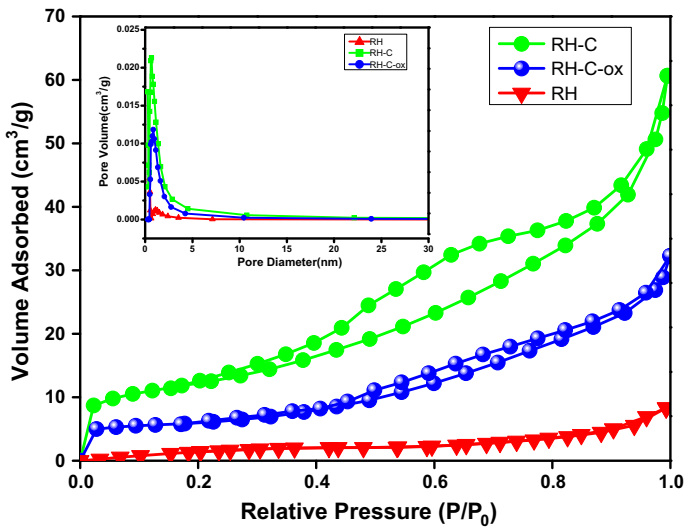


Fig. 2 N_2 adsorption–desorption isotherms and pore size distributions (*inset*) for RH, RH-C and RH-C-ox

Table 1 Specific surface area, average pore size and total pore volume of samples

Sample	RH	RH-C	RH-C-ox
Specific surface area ($m^2 g^{-1}$)	9.0	43.0	20.3
Pore volume ($cm^3 g^{-1}$)	0.01	0.11	0.06
Average pore diameter (nm)	8.3	5.9	6.9

Additionally, XPS analysis was applied to find the chemical binding in RH-C and RH-C-ox. The high resolution C_{1s} XPS spectra of the RH-C and RH-C-ox are shown in Fig. 4a, b, respectively. The spectrum of RH-C was resolved into two peaks with the binding energies at 286 and 287.2 eV, which are assigned to $C=C/O$ and $C=O$, respectively. Compared with RH-C, the C_{1s} region in the XPS spectrum of RH-C-ox exhibits a new peak at 290.1 eV, which is related to COOR (carboxylic groups of esters and/or lactones). As shown in Fig. 4c, d, the O_{1s} spectra of two samples are also distinctly observable. In the RH-C sample, the O_{1s} peak was deconvoluted to three major components with the binding energy peaks at 533.3, 534.5 and 535.8 eV, corresponding to the $C-O/C=O/O=C-O$, $C-O$, O/H_2O , respectively. However, in the RH-C-ox sample, the O_{1s} binding energy and intensity shifted slightly. As is reported, this can be related to variations in the charge density of oxygen in the valence band [43]. The peaks with binding energies of 533.7, 534.8 and 535.8 eV can be assigned to $C-O-C/SO_4^{2-}$, $Ph-O-(C=O)-O-Ph$ and O/H_2O , respectively, which reflect the variation and increment of the oxygen-containing functional groups onto the material. This demonstrates that more

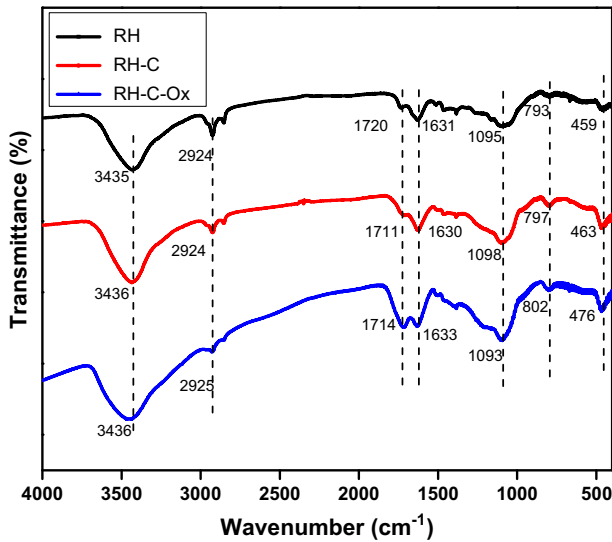


Fig. 3 FTIR spectra of the RH, RH-C and RH-C-ox

oxygenous functional groups were introduced during the surface oxidation process, which was also corroborated by the FTIR results.

Effect of pH on Pb(II) adsorption

As is known, solution pH is crucial for the adsorption process. Therefore, the effect of solution pH on the Pb(II) removal was firstly examined by varying the initial pH of the solutions from 2 to 6; the results are presented in Fig. 5. The removal efficiency of Pb(II) was low at a pH <3; this was due to the surplus protons competing with Pb(II) for the active sites. It is evident that the adsorption efficiency increased with increasing the pH from 2 to 5. This may be ascribed to the electrostatic attraction between the adsorbent and enhancement of Pb(II), which was caused by deprotonation of oxygen-containing functional groups. With pH values higher than 5.0, the decreasing trend was possibly due to the formation of soluble hydroxyl complexes [44, 45]. Hence, pH 5.0 was chosen as the optimum pH for further studies in order to avoid lead precipitation.

Effect of contact time and initial concentration

Figure 6 shows the effect of contact time on Pb(II) adsorption at different initial concentrations ranging from 10 to 40 mg L⁻¹. The adsorption capacity of Pb(II) on the RH-C-ox increased steeply with increasing contact time from the beginning to 5 min, which may be related to the available vacant adsorption sites at this stage, and it was much easier for Pb(II) to access these sites, resulting in a significantly rapid adsorption rate at the early stages. Thereafter, the adsorption uptake continued

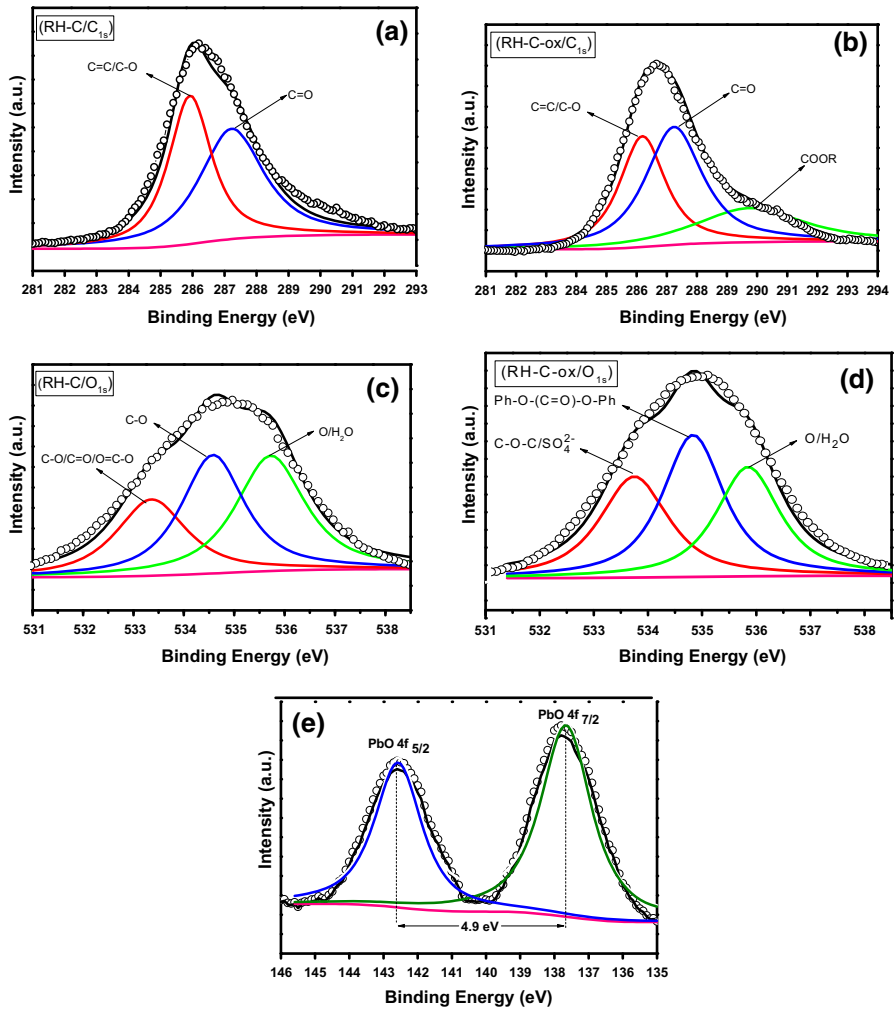


Fig. 4 XPS spectra of C_{1s} (a) RH-C; (b) RH-C-ox), O_{1s} (c) RH-C; (d) RH-C-ox), Pb 4f spectrum on RH-C-ox (e)

to increase at a slower rate and then reached equilibrium. This can be attributed to the saturation of the biosorption sites on RH-C-ox. It was found that equilibrium could be reached within 30 min, independent of the initial Pb(II) concentration. Hence, further experiments were adopted with 1.5 h as the proper contact time to ensure adsorption equilibrium. It was observed that the adsorption process was fast and that it could be easily achieved within 30 min. These results indicated that RH-C-ox can rapidly and efficiently remove Pb(II) from aqueous solution, owing to the direct electrostatic attraction [46, 47]. As is shown, the equilibrium adsorption capacity increased from 18.1 to 66.0 mg g⁻¹ when the concentration of Pb(II) increased from 10 to 40 mg L⁻¹. This is because a high concentration of Pb(II) can

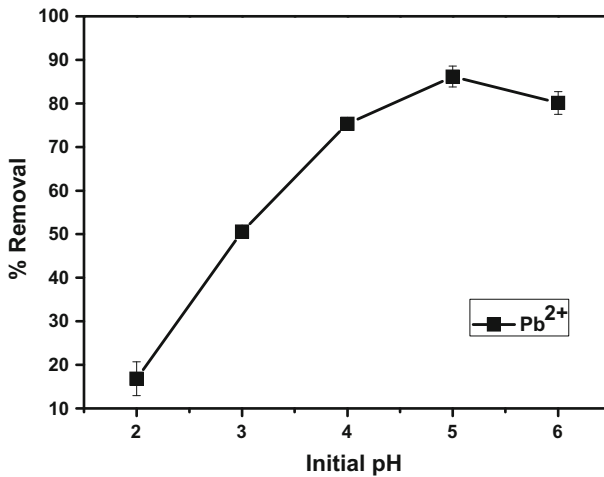


Fig. 5 Effect of the pH on the adsorption of Pb(II) onto RH-C-ox (adsorbent dose, 0.01 g; volume, 20 mL; initial Pb(II) concentration, 30 mg L⁻¹; contact time, 1.5 h; temperature, 298 ± 2 K)

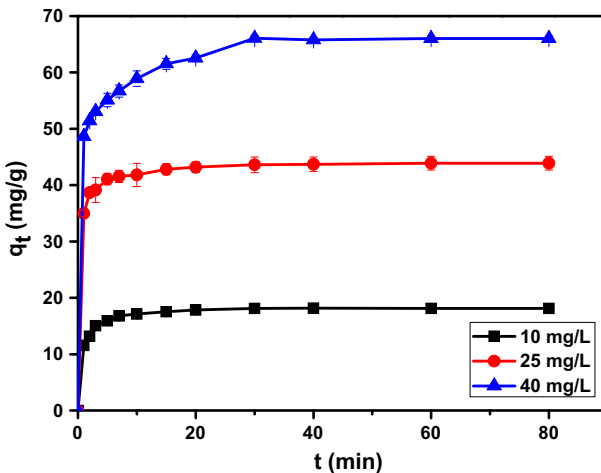
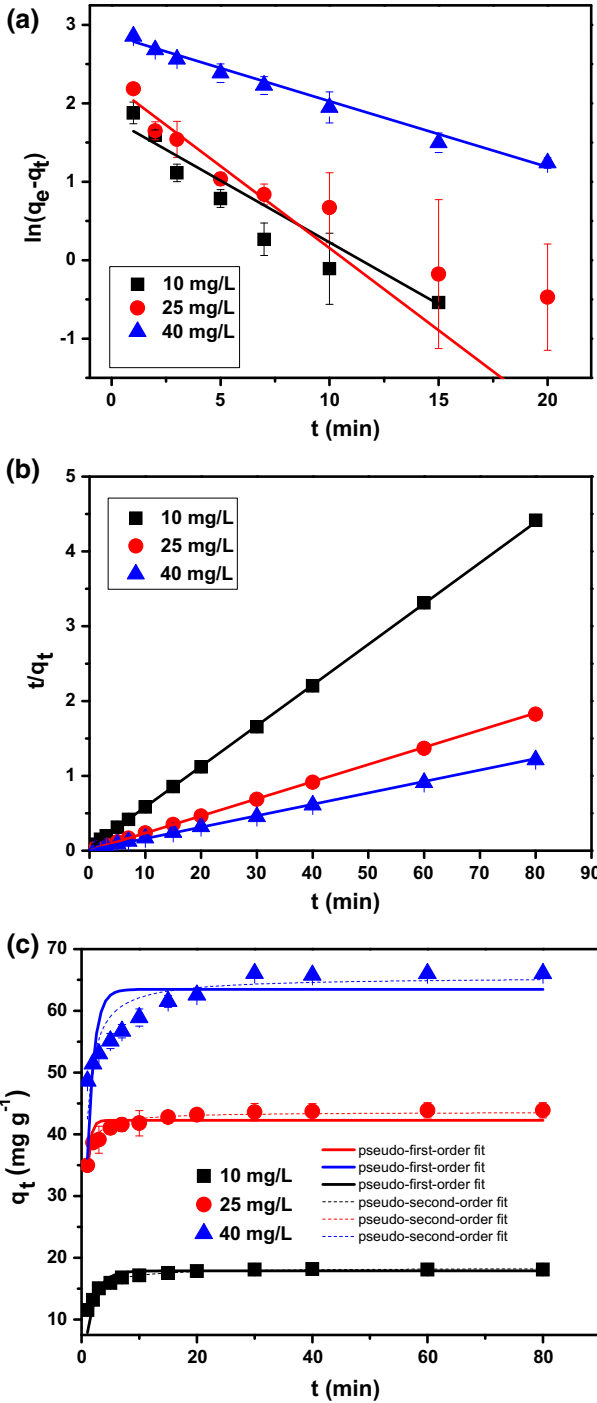


Fig. 6 Effect the contact time on Pb(II) adsorption at different initial concentrations of 10, 25 and 40 mg L⁻¹ (adsorbent dose, 0.01 g; volume, 20 mL; pH, 5.0; temperature, 298 ± 2 K)

serve as an important driving force to overcome all of the mass transfer resistance, contributing to higher adsorption capacity.

Adsorption kinetics

In order to gain insight into the mechanism of Pb(II) adsorption by RH-C-ox, a pseudo-first-order kinetic model and pseudo-second-order kinetic model were used to study the adsorption, which were expressed as follows [48]:



◀ **Fig. 7** Linear pseudo-first-order kinetic model (a), linear pseudo-second-order kinetic model (b), nonlinear pseudo first-order and pseudo second-order kinetic models (c) for adsorption of Pb(II) onto RH-C-ox

$$\ln(q_e - q_t) = \ln q_e - k_1 t \quad (5)$$

$$\frac{t}{q_t} = \frac{1}{k_2 q_e^2} + \frac{t}{q_e} \quad (6)$$

where q_e and q_t are the adsorption capacity of metal ions at equilibrium and at time t , respectively; k_1 (min^{-1}) and k_2 ($\text{g mg}^{-1} \text{min}^{-1}$) represent rate constants of the pseudo-first-order and pseudo-second-order models, respectively.

The corresponding nonlinear pseudo-first-order model and nonlinear pseudo-second-order kinetic model can be expressed as follows [34]:

$$Q_t = Q_e(1 - e^{-k_1 t}) \quad (7)$$

$$Q_t = \frac{t}{\frac{1}{k_2 Q_e^2} + \frac{t}{Q_e}} \quad (8)$$

Figure 7a, b shows the linear regression curves of $\ln(q_e - q_t)$ against t and t/q_t against t , respectively. The kinetic parameters were obtained from the slopes and intercepts (see Table 2). As can be seen from the results, the correlation coefficients of the pseudo-second-order model were much higher than those of the pseudo-first-order model. In addition, the $q_{e,\text{cal}}$ values by the fitting of the pseudo-second-order model were nearer to the experimental values. Therefore, indicating that the Pb(II) biosorption process is described by the pseudo-second-order model. This is consistent with the surface chemistry of the resulting carbon–silica composite bio-sorbent with plentiful and accessible oxygen-containing functional groups induced by the surface oxidization treatment. Also, the kinetic models for removal of Pb(II) using nonlinear regression is presented in Fig. 7c and the kinetic parameters determined by nonlinear regressions are given in Table 3. It can be seen that the pseudo-first-order kinetic model does not give a good fit, which was corroborated by a low R^2 and high SD (%). The data of the nonlinear fitting is consistent with the linear fitting, further indicating that the pseudo-second-order kinetic model is more suitable for describing the adsorption behavior of Pb(II) onto RH-C-ox.

At the same time, the dynamic adsorption behavior of RH-C for Pb(II) was also investigated (Fig. S1). Compared with RH-C-ox, RH-C possessed a much lower adsorption capacity, and the equilibrium adsorption capacities of RH-C were lower under each initial Pb(II) concentration than RH-C-ox. It is, thus, clearly revealed that oxidization treatment can significantly enhance the efficiency of sorbents, through which more surface oxygen sites were provided for contact with Pb(II). This was because the oxygen-containing functional groups increased the number of active sites which played a significant role on carbon–silica composite bio-sorbent adsorption. The efficiency of RH-C-ox was high after adding oxygen-containing functional groups on RH-C. Hence, it can be concluded that the oxidization treatment could increase the content of oxygen-containing functional groups, which

Table 2 Kinetic parameters for adsorption of Pb(II) onto RH-C-ox

Kinetic parameters	Initial concentrations (mg L ⁻¹)		
	10	25	40
$q_{e,exp}$ (mg g ⁻¹)	18.113	43.889	66.03
<i>Linear</i>			
Pseudo-first-order model			
$q_{e,cal}$ (mg g ⁻¹)	6.059	9.446	17.625
k_1 (min ⁻¹)	0.1574	0.2092	0.0841
R^2	0.9779	0.8747	0.9852
AIC	10.75	10.38	3.09
SD	65.52	80.60	73.15
Pseudo-second-order model			
$q_{e,cal}$ (mg g ⁻¹)	18.376	43.611	65.359
k_2 (g mg ⁻¹ min ⁻¹)	0.0771	0.0910	0.0289
R^2	0.9999	0.9999	0.9967
AIC	-6.31	-22.13	43.91
SD	23.30	9.50	17.11

Table 3 Adsorption kinetic constants and correlation coefficients for adsorption of Pb(II) onto RH-C-ox

Kinetic parameters	Initial concentrations (mg L ⁻¹)		
	10	25	40
<i>Nonlinear</i>			
Pseudo-first-order model			
$q_{e,cal}$ (mg g ⁻¹)	17.877	42.292	63.475
k_1 (min ⁻¹)	0.5833	1.6800	0.8409
R^2	0.7624	0.8353	0.7138
AIC	24.67	10.23	58.80
SD	21.03	7.73	14.69
Pseudo-second-order model			
$q_{e,cal}$ (mg g ⁻¹)	18.379	43.614	65.482
k_2 (g mg ⁻¹ min ⁻¹)	0.0766	0.0909	0.0282
R^2	0.9822	0.9893	0.9282
AIC	-6.42	-22.56	42.20
SD	23.32	9.50	17.28

could enhance lead removal efficiency. Also, it has been previously reported that oxygenous functional groups play an important role in the Pb(II) binding process [49]. The linear and nonlinear models were used to fit the dynamic adsorption data of Pb(II) on RH-C. According to Fig. S2 and Table S1, the dynamic adsorption of RH-C followed the pseudo-second-order model.

Adsorption isotherms

Figure 8 illustrates the adsorption isotherms of Pb(II) onto RH-C-ox at 293, 303 and 313 K. There is a clear trend that the adsorption capacity increased with increasing initial Pb(II) concentration, while a smaller change in adsorption capacity was observed as temperature increased, indicating that the temperature did not have a significant effect on the Pb(II) adsorption capacity. The experimental data were fitted with both Langmuir and Freundlich isotherm models [50, 51]. The two models can be expressed as follows:

$$\frac{C_e}{q_e} = \frac{C_e}{q_{\max}} + \frac{1}{q_{\max} \times b} \quad (9)$$

$$\log q_e = \log K_f + \frac{1}{n} \log C_e \quad (10)$$

where C_e is the equilibrium concentration (mg L^{-1}), q_e is the equilibrium adsorption capacity (mg g^{-1}), q_{\max} is the maximum single layer adsorption capacity (mg g^{-1}), and b is equilibrium constant (L mg^{-1}), K_f and n are adsorption constants related to adsorption capacity and adsorption intensity, respectively.

Besides, another parameter for the Langmuir isotherm is known as separation factor R_L , which is expressed as follows [52]:

$$R_L = \frac{1}{1 + bC_0} \quad (11)$$

where b is the Langmuir constant (L mg^{-1}) and C_0 is the initial adsorbate concentration (mg L^{-1}). The values of R_L are indicative of an adsorption process that

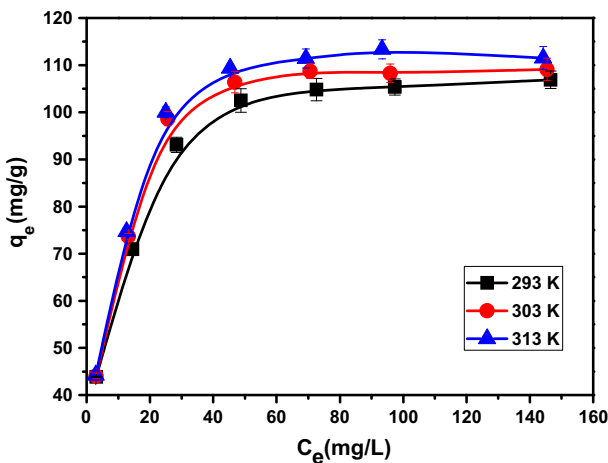
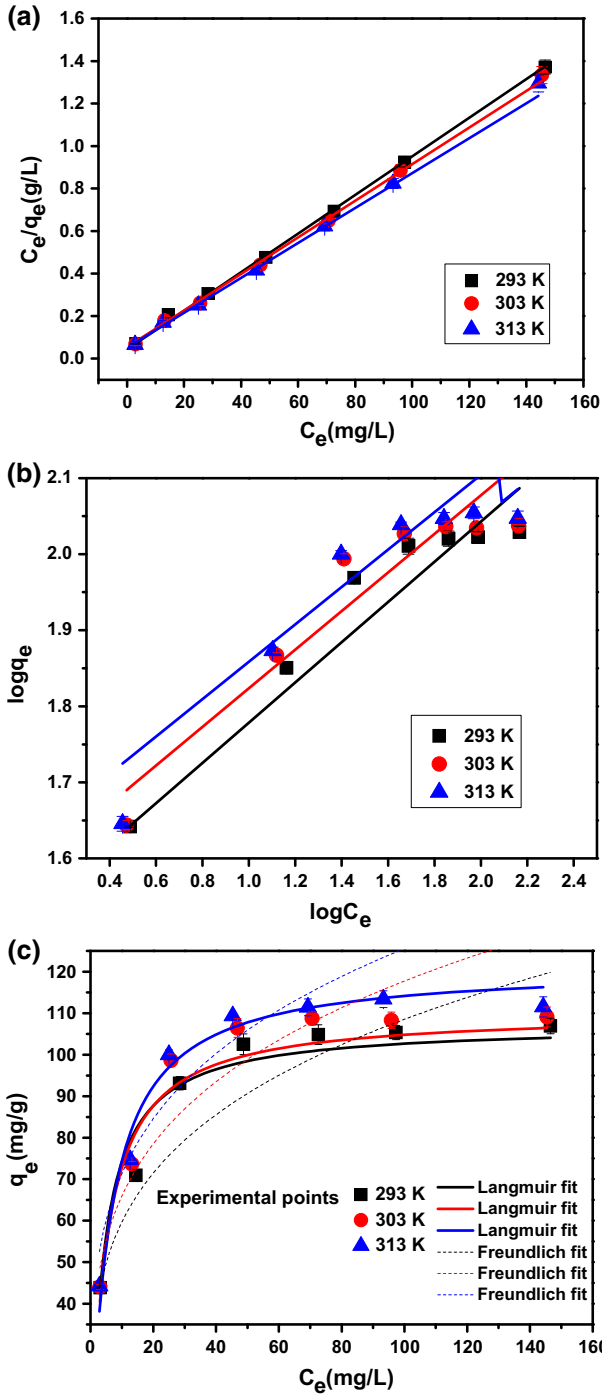


Fig. 8 Adsorption isotherms of Pb(II) onto RH-C-ox at different temperatures of 293, 303, and 313 (adsorbent dose, 0.01 g; volume, 20 mL; pH, 5.0 and contact time 1.5 h)



◀ **Fig. 9** Linear Langmuir (a) and Freundlich (b) isotherm plots, and non-linear Langmuir and Freundlich isotherm plots (c) for adsorption of Pb(II) onto RH-C-ox

might be irreversible ($R_L = 0$), favorable ($0 < R_L < 1$), linear ($R_L = 1$) or unfavorable ($R_L > 1$).

The linear plots of two isotherm models are presented in Fig. 9a, b, and the results of Langmuir and Freundlich parameters are summarized in Table 4. According to the correlation coefficients (R^2), the equilibrium data matched well with the Langmuir models, and the Langmuir model exhibited a much better fit than the Freundlich model, meaning that the adsorption of Pb(II) by RH-C-ox may be a monolayer adsorption. It is noticeable that all the R_L values were between 0 and 1; thus, the adsorption by RH-C-ox could be regarded as a favorable process. On the basis of the Langmuir isotherm model, the maximum adsorption capacity of Pb(II) on RH-C-ox is about 121.803 mg g⁻¹ at 313 K, which reveals that as-prepared carbon–silica composite RH-C-ox with designed surface chemistry is a potential bio-sorbent for efficient Pb(II) removal from an aqueous solution. In addition, non-linear Langmuir, Freundlich and D–R isotherm models were also tested, which can be expressed as follows [34]:

$$Q_e = \frac{Q_m K_L C_e}{1 + K_L C_e} \quad (12)$$

$$Q_e = K_F C_e^{\frac{1}{n}} \quad (13)$$

$$q_e = q_m \exp(-\beta \varepsilon^2) \quad (14)$$

$$E = \frac{1}{\sqrt{2\beta}}$$

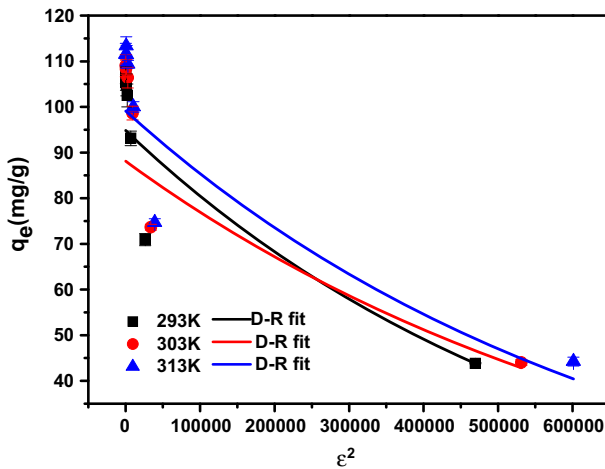
where Q_m or q_m (mg g⁻¹) is the maximum adsorption amount, ε is the Polanyi potential equal to $RT \ln(1 + (1/C_e))$, and β is the constant related to free energy E (J mol⁻¹).

The non-linear Langmuir, Freundlich and D–R isotherm curves are shown in Figs. 9c and 10. The estimated model parameters with the correlation coefficient (R^2), second-order corrected AIC and the SD (%) are listed in Table 5. It was found that the experimental data fitted the Langmuir isotherm better than the other two isotherms in terms of R^2 , AIC and SD values, which was more appropriate to describe the process of sorption by RH-C-ox, indicating the surface homogeneity of the adsorbent. Besides, the data of the nonlinear fitting is consistent with linear fitting. The isotherm data was fitted with the D–R model, and the values of E obtained were all lower than 8 kJ mol⁻¹, suggesting the adsorption process was related to physical adsorption.

The Pb(II) adsorption capacity of RH-C-ox is compared to those of other recently reported bio-sorbents obtained from agriculture wastes. It is apparent that the maximum adsorption capacity (q_{\max}) of adsorbent from this work is comparable or considerably greater than other reported bio-sorbents (Table 6) [53–57].

Table 4 Isotherm parameters for adsorption of Pb(II) onto RH-C-ox

Temperature (K)	Langmuir model				Freundlich model		
	q_m (mg g ⁻¹)	b (L mg ⁻¹)	R_L	R^2	K_f (L g ⁻¹)	$1/n$	R^2
293	110.011	0.2134	0.0229–0.1579	0.9983	32.652	0.2646	0.9765
303	116.279	0.1590	0.0305–0.2010	0.9956	37.140	0.2539	0.8982
313	121.803	0.1606	0.0302–0.1994	0.9955	41.013	0.2457	0.8282

**Fig. 10** DR isotherm plots for adsorption of Pb(II) onto RH-C-ox

Thermodynamic studies

To further study the thermodynamic behavior of Pb(II) adsorption by RH-C-ox, parameters such as Gibbs free energy change (ΔG^0), enthalpy change (ΔH^0) and entropy change (ΔS^0) were calculated using the following equation [58, 59]:

$$\Delta G^0 = -RT \ln K_d \quad (15)$$

$$K_d = \frac{q_e}{C_e} \quad (16)$$

$$\ln K_d = \frac{\Delta S^0}{R} - \frac{\Delta H^0}{RT} \quad (17)$$

where K_d is the equilibrium constant, R is the gas constant (8.314 J mol⁻¹ K⁻¹) and T is the absolute temperature.

Table 5 Adsorption isotherm constants and correlation coefficients for adsorption of Pb(II) at different temperatures

Isotherm	Temperature (K)			
	Parameters	293 K	303 K	313 K
Langmuir	$Q_m(\text{mg g}^{-1})$	107.229	110.171	121.325
	$K_L(\text{L mg}^{-1})$	0.2243	0.1948	0.1591
	R^2	0.9806	0.9455	0.9566
	AIC	20.99	26.49	23.92
	SD	24.00	22.86	30.60
Freundlich	$K_F(\text{L g}^{-1})$	32.82	36.93	40.55
	$1/n$	0.2596	0.2517	0.2454
	R^2	0.9560	0.9090	0.8749
	AIC	26.71	30.08	31.33
	SD	77.93	87.36	95.67
D-R	$q_m(\text{mg g}^{-1})$	94.883	88.135	99.135
	$E(\text{kJ mol}^{-1})$	0.551	0.607	0.579
	R^2	0.9193	0.7506	0.7068
	AIC	30.96	37.14	37.29
	SD	50.11	44.52	53.17

Table 6 Comparison of the Q_{\max} of Pb(II) between different bio-sorbents

Bio-sorbent	$q_{\max}(\text{mg g}^{-1})$	References
Sawdust	21.05	[53]
<i>Moringa oleifera</i> bark	34.60	[54]
<i>Polygonum orientale</i> linn	99.01	[55]
Pine cone activated carbon	27.53	[56]
Sulfured orange peel	164.00	[57]
Tartaric acid modified		
Rice husk	108	[30]
Rice husk ash	12.61	[31]
Carbon-silica composite	121.80	This work

The values of ΔH^0 and ΔS^0 were computed from the slope and intercept of the plot of $\ln K_d$ against $1/T$. The experimental results were represented in Fig. 11 and Table S2. The ΔH^0 values found for the adsorption of Pb(II) is positive, indicative of the endothermic nature of the adsorption process. The values of ΔG^0 are negative, illuminating that adsorption of Pb(II) onto RH-C-ox is a spontaneous process. The decrease in ΔG^0 with increasing temperature implies higher temperature favored the adsorption. The positive value of ΔS^0 reflects the increasing randomness at the adsorbent surface during the adsorption of Pb(II) ions onto RH-C-ox, which finally leads to enhanced adsorption capacity.

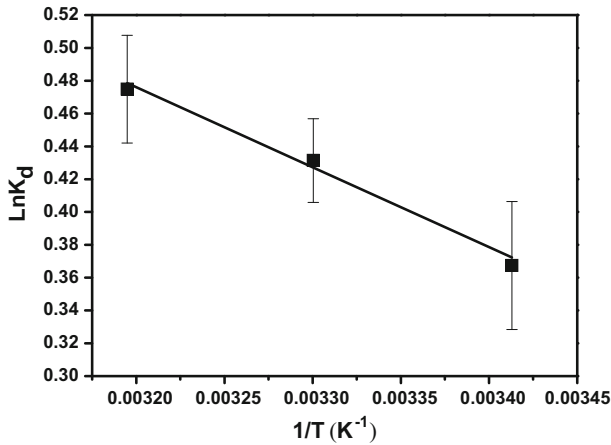


Fig. 11 Relationship curve between $\ln K_d$ and $1/T$

Effect of ionic strength on Pb(II) adsorption

It is well known that common wastewater usually contains several cations, which may affect the removal efficiency of Pb(II) to a certain extent. Thus, the effect of commonly coexisting ions on the removal of Pb(II) was studied by adding NaNO_3 and CaCl_2 at different concentrations. The relationship between Pb(II) removal percentage by RH-C-ox and ionic strength is shown in Fig. 12. It can be observed that the removal efficiency of Pb(II) decreases with increasing ionic strength, which suggests that the presence of the cations has a significant influence on the removal of

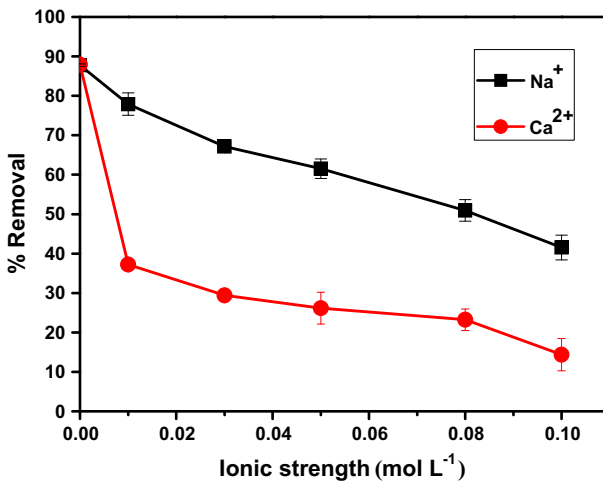


Fig. 12 Effect of ionic strength on Pb(II) removal (adsorption conditions: $C_0 = 25 \text{ mg L}^{-1}$; adsorbent dose, 0.01 g; volume, 20 mL; pH, 5.0; contact time, 1.5 h; temperature, $298 \pm 2 \text{ K}$)

Pb(II). This can be explained by the fact that the stronger ionic strength generated more Na^+ or Ca^{2+} ions that could occupy the active sites, accordingly increasing the electrostatic repulsion between adsorbent particles and adsorbates, which in turn constrained the amount of sorption sites for the sorption of Pb(II), thereby reducing the adsorption effectiveness.

Additionally, the presence of divalent Ca^{2+} has a greater negative effect on Pb(II) adsorption compared with that of Na^+ , this could be due to the fact that Ca^{2+} can screen more negative charges on RH-C-ox, thus exhibiting a lower adsorption capacity of Pb(II) than Na^+ . This is a favorable demonstration that there would be the existence of strong electrostatic interactions between Pb(II) and RH-C-ox.

Adsorption mechanism

The adsorption of Pb(II) onto the adsorbent can be considered as physical adsorption and electrostatic attraction; and electrostatic attraction is a major factor allowing the ions to approach the negatively charged surface of RH-C-ox. Also, XPS studies were conducted to further understand the adsorption mechanism of Pb(II) on RH-C-ox. The XPS spectrum of lead-loaded RH-C-ox is shown in Fig. 3e. The relevant Pb 4f photoelectron peak appears at the binding energies of 137.6 and 142.5 eV, corresponding to PbO 4f 7/2 and PbO 4f 5/2, respectively, which indicates that lead is bound on the RH-C-ox through oxygenous functional groups. This finding proves that it is oxygenous functional groups that played the dominant role in Pb(II) sorption under testing conditions.

Desorption and reusability

Considering the capability for practical or industrial applications, the reusability of adsorptive materials seems to be very important. For the evaluation of adsorbent reusability, regeneration experiments for RH-C-ox were carried out using 0.1 M HCl, and the regenerated RH-C-ox was examined for four consecutive cycles. As shown in Fig. 13, the removal efficiency is slightly reduced after each cycle, which is largely attributed to the loss of adsorbent amount. Nonetheless, a removal efficiency over 80 % can be maintained after four runs; this demonstrates that the resulting carbon–silica composite RH-C-ox, with plentiful and accessible oxygen-containing functional groups, has good reusability.

Conclusions

A new rice husk-based carbon–silica composite bio-sorbent was successfully prepared by employing a two-step method, i.e., firstly carbonization of rice husk with sulfuric acid and followed by surface oxidation treatment with ammonium persulfate solution. This method is simple, mild and controllable. The adsorption results revealed that Pb(II) adsorption followed the pseudo-second order model and Langmuir isotherm. Thermodynamic studies suggested that the adsorption process was spontaneous and endothermic. Furthermore, the desorption experiment showed

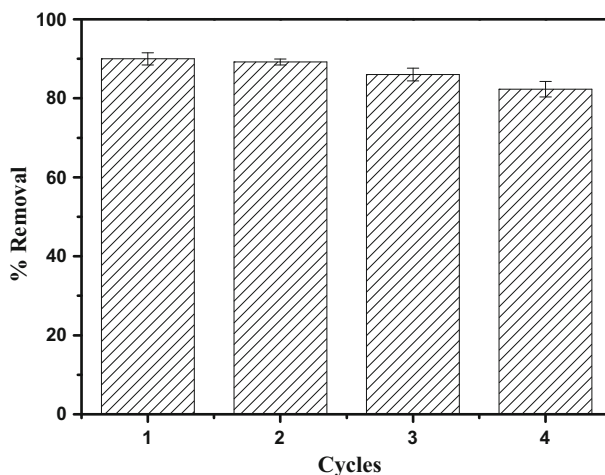


Fig. 13 Recycling performance during four successive cycles

that an adsorption performance of up to 80 % can be retained even after the sorbent was used four times. FTIR and XPS analyses revealed that oxygen-containing groups on the surface of RH-C-ox played a crucial role in lead adsorption. In view of the economical and environmental points, this renewable carbon–silica composite bio-sorbent has great potential to remove Pb(II) from practical wastewater as the sorbent is inexpensive, effective and environmentally safe.

Acknowledgments Financial support from the National Natural Science Foundation of China (21446001), the Program for Liaoning Innovative Research Team in University (LT2013012) and the Program for Liaoning Excellent Talents in University (LJQ2014056) is highly appreciated.

References

1. B.L. Martins, C.C.V. Cruz, A.S. Luna, C.A. Henriques, *Biochem. Eng. J.* **27**, 310 (2006)
2. L.J. Dong, Z.L. Zhu, Y.L. Qiu, J.F. Zhao, *Chem. Eng. J.* **165**, 827 (2010)
3. A. Mishra, A. Malik, *Water Res.* **46**, 4991 (2012)
4. F. Aydın, F. Yasar, I. Aydın, F. Guzel, *Microchem. J.* **98**, 246 (2011)
5. I. Hajdu, M. Bodnár, Z. Csikós, S. Wei, L. Daróczy, B. Kovács, Z. Győri, J. Tamás, J. Borbély, *J. Membr. Sci.* **409–410**, 44 (2012)
6. F.M. Pang, P. Kumar, T.T. Teng, A.K.M. Omar, K.L. Wasewar, *J. Taiwan Inst. Chem. Eng.* **42**, 809 (2011)
7. W.F. Liu, Z.P. Zhao, Y.Q. Guo, *Chin. J. Chem. Eng.* **21**, 227 (2013)
8. Y. Bulut, Z. Baysal, *J. Environ. Manag.* **78**, 107 (2006)
9. S. Schiewer, S.B. Patil, *Bioresour. Technol.* **99**, 1896 (2008)
10. A.E. Ofomaja, E.I. Unuabonath, N.A. Oladoja, *Bioresour. Technol.* **101**, 3844 (2010)
11. O.D. Uluozlu, A. Sari, M. Tuzen, M. Soylak, *Bioresour. Technol.* **99**, 2972 (2008)
12. R.A. Anayurt, A. Sari, M. Tuzen, *Chem. Eng. J.* **151**, 255 (2009)
13. A. Sari, M. Tuzen, *J. Hazard. Mater.* **164**, 1004 (2009)
14. K.G. Mansaray, A.E. Ghaly, *Energy Sources* **20**, 653 (1998)
15. W. Arayaprance, N. Na-Ranong, G.L. Rempel, *J. Appl. Polym. Sci.* **98**, 34 (2005)

16. F.A. Services *Grain: World Markets and Trade*. (United States Department of Agriculture, 2013)
17. Y. Chen, Y.C. Zhu, Z.C. Wang, Y. Li, L.L. Wang, L.L. Ding, X.Y. Gao, Y.J. Ma, Y.P. Guo, *Adv. Colloid Interface Sci.* **163**, 39 (2011)
18. M. Fang, L. Yang, G. Chen, Z. Shi, Z. Luo, K. Cen, *Fuel Process. Technol.* **85**, 1273 (2004)
19. J.L. Zheng, *J. Anal. Appl. Pyrolysis* **80**, 30 (2007)
20. F. Duan, C.S. Chyang, C.W. Lin, J. Tso, *Bioresour. Technol.* **134**, 204 (2013)
21. S. Kamenidou, T.J. Cavins, S. Marek, *Sci. Hortic.* **123**, 390 (2010)
22. G.R. de Sensale, *Cem. Concr. Compos.* **28**, 158 (2006)
23. C.Y. Lu, M.Y. Wey, K.H. Chuang, *Appl. Catal. B Environ.* **90**, 652 (2009)
24. Y.P. Guo, J.R. Qi, Y.Q. Jiang, S.F. Yang, Z.C. Wang, H.D. Xu, *Mater. Chem. Phys.* **80**, 704 (2003)
25. D.P. Wong, R. Suriyaprabha, R. Yuvakumar, V. Rajendran, Y.T. Chen, B.J. Hwang, L.C. Chen, K.H. Chen, *J. Mater. Chem. A*, **2**, 13437 (2014)
26. L.P. Wang, Z. Schnepp, M.M. Titirici, *J. Mater. Chem. A* **1**, 5269 (2013)
27. D. Roy, P.N. Greenlaw, B.S. Shane, *J. Environ. Sci. Health* **28**, 37 (1993)
28. E. Munaf, R. Zein, *Environ. Technol.* **18**, 359 (1997)
29. Y.P. Guo, J.R. Qi, S.F. Yang, K.F. Yu, Z.C. Wang, H.D. Xu, *Mater. Chem. Phys.* **78**, 1–32 (2003)
30. K.K. Wong, C.K. Lee, K.S. Low, M.J. Haron, *Chemosphere* **50**, 23 (2003)
31. Q.G. Feng, Q.Y. Lin, F.Z. Gong, S. Sugita, M. Shoya, *J. Colloid Interface Sci.* **278**, 1 (2004)
32. C.R.T. Tarley, S.L.C. Ferreira, M.A.Z. Arruda, *Microchem. J.* **77**, 163 (2004)
33. H.P. Ye, Q. Zhu, D.Y. Du, *Bioresour. Technol.* **101**, 5175 (2010)
34. J.H. Zhang, H. Fu, X.S. Lv, J. Tang, X.H. Xu, *Biomass Bioenergy* **35**, 464 (2011)
35. Z.G. Liu, F.S. Zhang, *Desalination* **267**, 101 (2011)
36. L. Lin, S.R. Zhai, Z.Y. Xiao, Y. Song, Q.D. An, X.W. Song, *Bioresour. Technol.* **136**, 437 (2013)
37. Y. Chen, S.R. Zhai, N. Liu, Y. Song, Q.D. An, X.W. Song, *Bioresour. Technol.* **144**, 401–409 (2013)
38. E.I. El-Shafey, *J. Hazard. Mater.* **147**, 546 (2007)
39. M. Hadi, M.R. Samarghandi, G. McKay, *Chem. Eng. J.* **160**, 408 (2010)
40. K.P. Burnham, D.R. Anderson, K.P. Huyvaert, *Behav. Ecol. Sociobiol.* **65**, 23 (2011)
41. F. Adam, J.H. Chua, *J. Colloid Interface Sci.* **280**, 55 (2004)
42. T.H. Liou, S.J. Wu, *J. Hazard. Mater.* **171**, 693 (2009)
43. P.S. Bagus, C.W. Bauschlicher, *J. Electron Spectrosc. Relat. Phenom.* **20**, 183 (1980)
44. I. Kula, M. Uğurlu, H. Karaoğlu, A. Çelik, *Bioresour. Technol.* **99**, 492 (2008)
45. G. Blázquez, F. Hernáinz, M. Calero, L.F. Ruiz-Núñez, *Process Biochem.* **40**, 2649 (2005)
46. K.K. Krishnani, X.G. Meng, C. Christodoulatos, V.M. Boddu, *J. Hazard. Mater.* **153**, 1222 (2008)
47. X.Y. Xu, X.D. Cao, L. Zhao, H.J. Zhou, Q.S. Luo, *RSC Adv.* **4**, 44930 (2014)
48. H. Guo, S.F. Zhang, Z.N. Kou, S.R. Zhai, W. Ma, Y. Yang, *Carbohydr. Polym.* **115**, 1–77 (2015)
49. Z.G. Liu, F.S. Zhang, *J. Hazard. Mater.* **167**, 933 (2009)
50. I. Langmuir, *J. Am. Chem. Soc.* **38**, 2221 (1916)
51. H. Freundlich, *Z. Phys. Chem.* **57**, 385 (1906)
52. K.R. Hall, L.C. Eagleton, A. Acrivos, T. Vermeulen, *Ind. Eng. Chem. Fundam.* **5**, 212 (1966)
53. Q. Li, J.P. Zhai, W.Y. Zhang, M.M. Wang, J. Zhou, *J. Hazard. Mater.* **141**, 163 (2007)
54. D.H.K. Reddy, K. Seshiah, A.V.R. Reddy, M.M. Rao, M.C. Wang, *J. Hazard. Mater.* **174**, 831 (2010)
55. L. Wang, J. Zhang, R. Zhao, Y. Li, C. Li, C.L. Zhang, *Bioresour. Technol.* **101**, 5808 (2010)
56. M. Momčilović, M. Purenović, A. Bojić, A. Zarubica, M. Randelović, *Desalination* **276**, 53 (2011)
57. S. Liang, X.Y. Guo, Q.H. Tian, *Desalination* **275**, 212 (2011)
58. A. Sari, D. Mendil, M. Tuzen, M. Soylak, *Chem. Eng. J.* **144**, 1 (2008)
59. A. Sari, M. Tuzen, *J. Hazard. Mater.* **160**, 349 (2008)